fluids

MDPI

Article

Experimental and Numerical Investigation of Drag Reduction and Heat-Transfer Characteristics of Xanthan Gum Solutions at Different Concentrations in Turbulent Pipe Flow Under Varying Temperature Conditions

Andi Cahya Ichi [1], Sri Poernomo Sari [2,*], Gunawan [1] and Yanuar [1]

[1] Department of Mechanical Engineering, University of Indonesia, Jakarta 16424, Indonesia; andiichi31@gmail.com (A.C.I.); gunawan_kapal@ui.ac.id (G.); yanuar@eng.ui.ac.id (Y.)
[2] Department of Mechanical Engineering, Gunadarma University, Jakarta 16424, Indonesia
* Correspondence: sri_ps@staff.gunadarma.ac.id

Abstract

This study presents a combined experimental and numerical investigation of xanthan gum solutions at 100 and 300 ppm in turbulent smooth pipe flow under temperatures of 30–50 °C and Reynolds numbers of 8000–12,000. Water was used as the Newtonian reference fluid, while xanthan gum was modelled using temperature- and concentration-dependent shear-thinning properties. Experimental pressure-drop data were used to evaluate drag-reduction behaviour, whereas numerical simulations were employed to analyse the associated flow and heat-transfer responses. The results show that XG 100 ppm produced a relatively stable drag-reduction response of approximately 31–39%, while XG 300 ppm showed a wider and more condition-dependent range of about 25–45%. Water exhibited higher Nusselt numbers of approximately 68–106. In contrast, XG 100 ppm produced Nusselt numbers of approximately 45–69, while XG 300 ppm showed lower values of about 35–61. The corresponding heat-transfer reduction ranged from approximately 26–48% for XG 100 ppm and 23–46% for XG 300 ppm. These findings confirm a clear hydraulic–thermal trade-off, indicating that the xanthan gum concentration should be optimised according to both pressure-loss reduction and heat-transfer requirements.

Keywords: computational fluid dynamics; xanthan gum; drag reduction; heat-transfer reduction; Nusselt number; non-Newtonian fluid; temperature effect

Check for updates

Academic Editors: Nilanjan Chakraborty, Chengcheng Tao and Mehrdad Massoudi

Received: 7 April 2026
Revised: 25 May 2026
Accepted: 2 June 2026
Published: 16 June 2026

Copyright: © 2026 by the authors. Licensee MDPI, Basel, Switzerland. This article is an open access article distributed under the terms and conditions of the Creative Commons Attribution (CC BY) license.

1. Introduction

Pressure loss and heat-transfer performance are two important aspects in internal flow systems, particularly in industrial applications involving fluid transport and thermal exchange. In pipe flow, frictional resistance increases the pumping power requirements, while the thermal performance of the fluid determines the effectiveness of heat transfer. Therefore, any attempt to improve hydraulic efficiency must also consider its possible influence on heat-transfer behaviour [1].

One of the most widely studied methods for reducing frictional resistance is the addition of drag-reducing agents into the base fluid. Polymer additives, even at low concentrations, are known to suppress flow resistance and reduce pressure drop. Among these additives, xanthan gum has attracted attention because it is water-soluble, effective at relatively low concentrations, and exhibits non-Newtonian shear-thinning behaviours.

These characteristics make xanthan gum a promising candidate for improving hydraulic performance in internal flow systems [2–6].

Unlike water, which behaves as a Newtonian fluid at a given temperature, xanthan gum solution exhibits an apparent viscosity that varies with shear rate. This non-Newtonian behaviour affects the velocity gradient, wall shear stress, friction factor, and pressure drop. At the same time, the presence of polymer additives may also alter the convective heat-transfer performance of the fluid. In many drag-reducing flows, the reduction in momentum transfer is often accompanied by a reduction in heat-transfer rate, creating a trade-off between hydraulic benefit and thermal penalty [7–12].

Temperature is another key factor governing the behaviours of both water and xanthan gum solution. For water, an increasing temperature generally lowers the viscosity and changes both flow-resistance and heat-transfer characteristics. For the xanthan gum solution, temperature influences not only the viscosity but also its rheological response, which may further affect drag reduction and heat-transfer reduction. Therefore, the combined effect of temperature and polymer addition must be carefully evaluated to understand the overall flow and thermal performance [7–9,13,14].

Although polymer drag reduction and the rheological behaviour of xanthan gum have been widely investigated, the concentration-dependent coupling between hydraulic benefit and thermal penalty remains insufficiently clarified, particularly for dilute xanthan gum solutions under controlled temperature conditions [2,3,5–7,9,11,15,16]. Previous studies have commonly focused on drag reduction, rheological characterization, mixed-polymer systems, or pressure-loss prediction, while fewer works have simultaneously evaluated drag reduction, heat-transfer reduction, and temperature-dependent non-Newtonian behaviour within the same framework [7,9,17–21]. As a result, the combined influence of xanthan gum concentration and temperature on pressure drop, frictional resistance, Nusselt number, and heat-transfer degradation requires further investigation. The research Summary present in Table 1.

Table 1. Research summary.

Researcher(s) and Year	Geometry Studied	Method	Main Findings	Limitation
Kadhim & Mahdy (2023) [5]	Horizontal cir-cular pipe	Experimental + CFD (COM-SOL)	Investigated rigid/modified xanthan gum systems and found reduced pressure drop and altered velocity/shear characteristics; the CFD re-sults supported the observed hydraulic behaviour.	Used modified or rigid xanthan gum mixtures rather than con-ventional aqueous xanthan gum solution; direct comparison with water and temperature-specific analysis remained limited
Habibpour & Clark (2017) [22]	Smooth circular pipe (turbulent flow)	Experimental)	Showed that hydrolyzed polyacrylamide/xanthan gum mixed polymer solutions can provide substantial drag re-duction, while xanthan gum improved shear resistance of the additive system.	Framed mainly as a mixed-polymer study rather than a pure xanthan gum study; did not systematically isolate the be-haviour of single-component XG over fixed thermal conditions.

Table 1. *Cont.*

Researcher(s) and Year	Geometry Studied	Method	Main Findings	Limitation
Ihmoudah et al. (2018) [23]	Circular pipe (horizontal vs. vertical)	Experimental + CFD (RANS)	Compared measured fric-tional pressure losses of xan-than-gum-based shear-thinning fluids with CFD predictions and dis-cussed how concentration affected agreement and hy-draulic behaviour.	Focused on drag-reducing polymer solution in general; did not specifically evaluate xanthan gum at 100 and 300 ppm under temperature variations of 30, 40, and 50 °C using combined experimental and CFD analysis.
Ogata et al. [24]	Circular tube/internal flow heat-transfer system	Experimental	Demonstrated the trade-off between drag reduction and heat-transfer reduction using xanthan gum, surfactant, and guar gum, and presented DR–HDR/HTR performance relationships.	The work was experimental and comparative across additives; it did not provide a temperature-specific numerical analysis of 100 ppm xanthan gum versus water.

To address this gap, the present study investigates the drag-reduction and heat-transfer characteristics of xanthan gum solutions at 100 and 300 ppm in turbulent smooth pipe flows at 30 °C, 40 °C, and 50 °C. Experimental pressure-drop measurements were used to evaluate and validate the drag-reduction behaviours, while numerical simulations were employed to analyze the associated flow and thermal responses under identical operating conditions. This combined experimental–numerical approach is important because xanthan gum rheology is strongly influenced by concentration and temperature, and CFD predictions of non-Newtonian turbulent flow are sensitive to the adopted rheological model and near-wall treatment [7,9,17–21]. The novelty of this study lies in evaluating concentration-dependent xanthan gum performance by linking the hydraulic advantage of drag reduction with its associated heat-transfer penalty [2,5,11,14].

2. Experimental and Numerical Procedures

2.1. Experimental Procedure

To facilitate understanding of the experimental configuration, Figure 1 presents a schematic diagram of the closed-loop pipe-flow system employed in this study.

The experimental investigation was conducted in a closed-loop pipe-flow system to obtain the pressure-drop characteristics of water and xanthan gum solutions at concentrations of 100 and 300 ppm. The test section consisted of a smooth circular pipe with an inner diameter of 8 mm and an effective pressure-drop measurement length of 0.8 m. The experiments were performed at controlled fluid temperatures of 30 °C, 40 °C, and 50 °C, over a Reynolds number range of 8000–12,000. Water was used as the Newtonian reference fluid, while xanthan gum solutions were prepared at the prescribed concentrations to evaluate the effect of polymer addition on drag reduction.

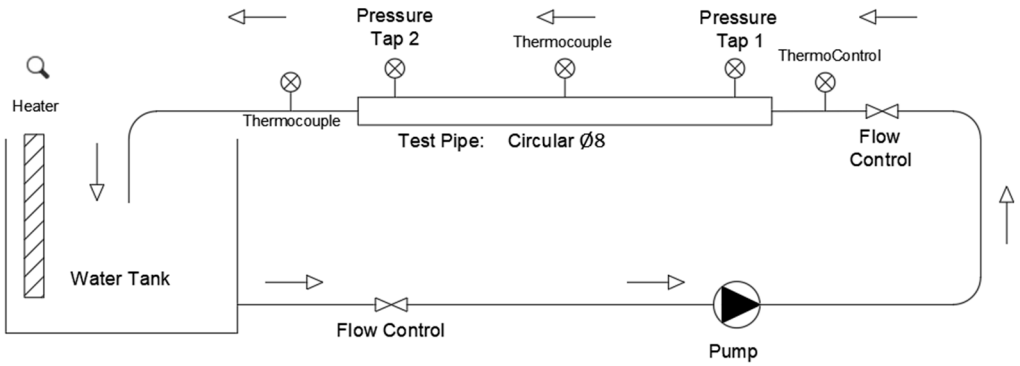


Figure 1. Schematic diagram of the closed-loop experimental pipe-flow system used for pressure-drop and heat-transfer measurements.

For water, the Reynolds number was calculated using the Newtonian definition:

$$Re = \frac{\rho V D}{\mu} \tag{1}$$

For xanthan gum solutions, the generalised Reynolds number for power-law fluids was used:

$$Re = \frac{\rho V^{2-n} D^n}{K\, 8^{n-1} \left(\frac{3n+1}{4n}\right)^n} \tag{2}$$

where ρ is the fluid density, V is the mean velocity, D is the pipe diameter, μ is the dynamic viscosity of water, K is the consistency index, and n is the flow behaviour index.

The pressure drop was measured between two pressure taps installed along the test section. The target Reynolds number was achieved by regulating the volumetric flow rate using the pump and flow-control valves in the closed-loop system. Thermocouples were used to monitor the fluid temperature during the experiment. The heater was regulated by a temperature-control unit to maintain the target fluid temperatures, and data acquisition was performed after the flow and thermal conditions reached a steady state.

2.2. Numerical Procedure

The xanthan gum solution was modelled as a non-Newtonian shear-thinning fluid using a power-law constitutive equation:

$$\tau = K\, \dot{\gamma}^n \tag{3}$$

where τ is the shear stress, $\dot{\gamma}$ is the shear rate, K is the consistency index, and n is the flow behaviour index. The K and n values used in the CFD simulations were estimated by fitting the shear-rate-dependent viscosity trend reported by Choppe et al. [7] to the power-law model; the fitted parameters were further adjusted and checked against the present experimental pressure-drop data to ensure consistency with the hydraulic behaviour observed in this study [21,25] The fitted power-law parameters, K and n, used in the CFD simulations are presented in Table 2.

The numerical domain consisted of a smooth circular pipe with an inner diameter of 8 mm and a length of 0.8 m. Water was used as the reference Newtonian fluid, while xanthan gum solutions at 100 and 300 ppm were modelled as a non-Newtonian fluid. Simulations were performed at 30 °C, 40 °C, and 50 °C for both fluids. The computational mesh used in the present study, including the cross-sectional mesh distribution with near-wall inflation layers and the longitudinal mesh distribution along the pipe, is shown in Figure 2.

Table 2. Fitted power-law rheological parameters of xanthan gum solutions used in the CFD simulations.

Fluid	Temperature (°C)	K (Pa·s^n)	*n*
XG 100 ppm	30	0.0119	0.876
	40	0.0104	0.859
	50	0.00969	0.813
XG 300 ppm	30	0.0710	0.689
	40	0.0616	0.653
	50	0.0561	0.609

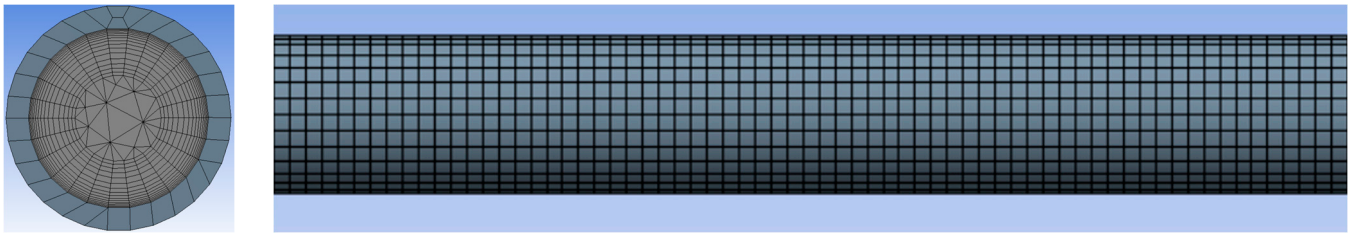


Figure 2. Computational mesh used in the present study: cross-sectional mesh distribution with near-wall inflation layers, and longitudinal mesh distribution along the pipe.

The domain was discretized using an unstructured patch-conforming mesh generated in ANSYS Meshing with curvature-based sizing and near-wall inflation. The mesh settings included a relevance value of 40, curvature-based advanced sizing, a minimum mesh size of 2.4662×10^{-4} m, and a growth rate of 1.2. The final mesh consisted of 1,061,197 nodes and 2,134,900 elements. Mesh independence was verified by comparing the predicted pressure drop and Nusselt number for several mesh configurations, and the final mesh was selected because further refinement produced negligible changes in the monitored parameters.

2.3. Solution Method

The flow and heat-transfer behaviour were numerically simulated using a computational fluid dynamics (CFD) approach based on the finite volume method [25–29]. The governing framework consisted of the steady-state conservation equations of mass, momentum, and energy for an incompressible fluid. The continuity equation is given by

$$\nabla \cdot u = 0 \tag{4}$$

where u is the velocity vector. The momentum equation is expressed as

$$\rho(u \cdot \nabla)u = -\nabla p + \nabla \cdot \tau \tag{5}$$

where ρ is the fluid density, p is the static pressure, and τ is the shear stress tensor. The thermal field was calculated using the energy equation:

$$\rho c_p(u \cdot \nabla\, T) = \nabla \cdot (k \nabla\, T) \tag{6}$$

To describe the turbulent flow behaviour, the shear stress transport (*SST*) k–ω turbulence model was employed because it provides good near-wall accuracy and stable prediction in the core flow region. In this study, Equation (7) represents the general finite-volume transport equation, whereas Equations (8) and (9) are the specific transport equations for turbulent kinetic energy k and specific dissipation rate ω in the *SST* k–ω model. Since the present simulations were performed under a steady-state RANS framework, the transient

terms in the turbulence transport equations were omitted in the numerical solution. The general transport equation solved in the finite volume method can be written as

$$\frac{\partial(\rho\phi)}{\partial t} + \nabla \cdot (\rho u \phi) = \nabla \cdot (\Gamma \phi \nabla \phi) + S\phi \tag{7}$$

where ϕ denotes the dependent variable, $\Gamma\phi$ is the diffusion coefficient, and $S\phi$ is the source term. For the *SST* k–ω model, the transport equation for turbulent kinetic energy k is given by

$$\frac{\partial(\rho k)}{\partial t} + \frac{\partial(\rho u_i k)}{\partial x_i} = \frac{\partial}{\partial x_j}\left[\left(\mu + \frac{\mu_t}{\sigma_k}\right)\frac{\partial k}{\partial x_j}\right] + G_k - Y_k \tag{8}$$

and the transport equation for the specific dissipation rate ω is expressed as

$$\frac{\partial(\rho\omega)}{\partial t} + \frac{\partial(\rho\omega_i k)}{\partial x_i} = \frac{\partial}{\partial x_j}\left[\left(\mu + \frac{\mu_t}{\sigma_k}\right)\frac{\partial \omega}{\partial x_j}\right] + G_w - Y_w + D_\omega \tag{9}$$

The turbulent viscosity is defined as

$$\mu t = \frac{\rho a 1 k}{max(a_1\omega, SF_2)} \tag{10}$$

where G_k and G_ω are the generation terms of the turbulent kinetic energy and specific dissipation rate, respectively, Y_k and Y_ω are the dissipation terms, D_ω is the cross-diffusion term, S is the strain rate magnitude, and F_2 is the blending function of the *SST* model.

$$G_k = \mu_t \, S^2 \tag{11}$$

$$Y_k = \rho \, \beta \, k \, \omega \tag{12}$$

$$G_\omega = \alpha \frac{\omega}{k} \, G_k \tag{13}$$

$$Y_w = \rho \, \beta \, \omega^2 \tag{14}$$

$$D_\omega = 2(1 - F_1)\rho \, \sigma \, \omega^2 \frac{1}{\omega} \, \frac{\partial k}{\partial x_j} \, \frac{\partial w}{\partial x_j} \tag{15}$$

where μ_t is the turbulent viscosity, S is the strain rate magnitude, ρ is the fluid density, and F_1 is the blending function of the *SST* model.

2.4. Solution Method Setting

The simulations were conducted using a pressure-based solver with the SIMPLE algorithm for pressure–velocity coupling. The gradient term was discretized using the least squares cell-based method, while the pressure and momentum equations were solved using the Second-Order and Second-Order Upwind schemes, respectively. The transport equations of turbulent kinetic energy and specific dissipation rates in the *SST* k–ω model were discretized using the First-Order Upwind scheme [21,26].

The convergence of the numerical solution was assessed from the residual histories and the stability of the monitored hydraulic and thermal parameters, particularly the pressure drop and Nusselt number, following conventional CFD convergence practice [21,26]. The *SST* k–ω model was adopted because it provides reliable near-wall treatment while maintaining stable prediction in the core flow region. In the present mesh, the area-weighted average wall y^+ was stable at approximately 1.3–1.6, indicating that the near-wall region was resolved consistently with the near-wall resolution requirement of the *SST* k–ω model.

Therefore, the adopted mesh and turbulence model were considered suitable for the present internal turbulent flow simulation involving wall shear and heat-transfer effects.

2.5. Boundary Conditions

A velocity inlet boundary condition was imposed at the pipe entrance, and the inlet velocity was varied according to the target Reynolds number for each simulation case. The turbulence quantities at the inlet were specified using the intensity and hydraulic diameter method, with a turbulence intensity of 5% and a hydraulic diameter of 0.008 m. At the outlet, a pressure outlet boundary condition was applied. The pipe wall was treated as a no-slip boundary for the flow field.

For the thermal analysis, the pipe wall was subjected to a constant heat flux of 4200 W/m^2. The wall material was assigned as acrylic, while the inlet fluid temperature was set to 30, 40, or 50 °C, depending on the simulation case. The same boundary-condition framework was applied to both water and xanthan gum solution to ensure a direct comparison of hydraulic and thermal performance.

The hydraulic and thermal performances of xanthan gum solution were evaluated relative to water under identical operating conditions. The drag reduction was calculated as

$$DR(\%) = \frac{\Delta P_{water} - \Delta P_{XG}}{\Delta P_{water}} \times 100 \quad (16)$$

while the heat-transfer reduction was determined from the Nusselt number as

$$HTR(\%) = \frac{Nu_{water} - Nu_{XG}}{Nu_{water}} \times 100 \quad (17)$$

where ΔP_{water} and ΔP_{XG} are the pressure drops of water and xanthan gum solution, respectively, and Nu_{water} and Nu_{XG} represent the corresponding Nusselt numbers.

Based on the numerical simulation procedure described above, the hydraulic and thermal responses of water and xanthan gum solutions at 100 and 300 ppm can be systematically evaluated under identical operating conditions. The resulting pressure drop, friction factor, drag reduction, Nusselt number, and heat-transfer reduction are presented and discussed in the following section.

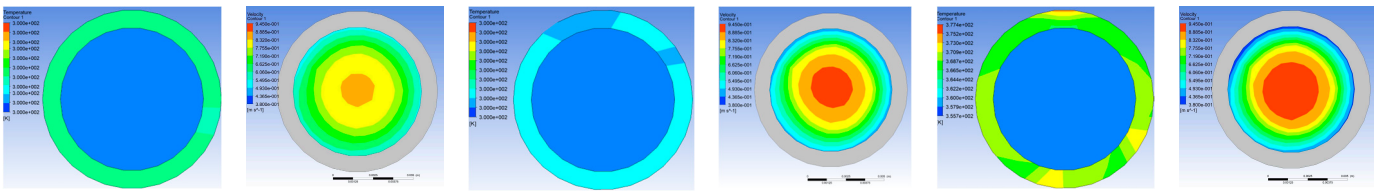
The present study considers two xanthan gum concentrations, namely 100 and 300 ppm, to evaluate the influence of polymer concentration on the coupled hydraulic and thermal behaviour. By maintaining the same pipe geometry, temperature range, and Reynolds number range, the effect of xanthan gum concentration can be isolated without introducing additional geometric variables. This study aims to provide a clear and controlled evaluation of temperature-dependent rheological effects on drag reduction and heat-transfer characteristics without introducing additional variables that may obscure the underlying physical mechanisms.

3. Results and Discussion

The hydraulic and thermal characteristics of the flow were initially examined through the cross-sectional contours of velocity and temperature for water and xanthan gum solutions at 100 and 300 ppm at 50 °C and Re = 10,000, as shown in Figure 3. The comparison provides a representative visualisation of how the rheological difference between the two fluids influences the internal flow and heat-transfer behaviour.

The velocity contours show that both fluids developed a high-velocity core and a lower-velocity region near the pipe wall due to the no-slip condition. However, the xanthan gum solution exhibited a different velocity distribution compared with water, indicating

that its non-Newtonian shear-thinning behaviour modified the wall-bounded momentum transport and the resulting flow structure.



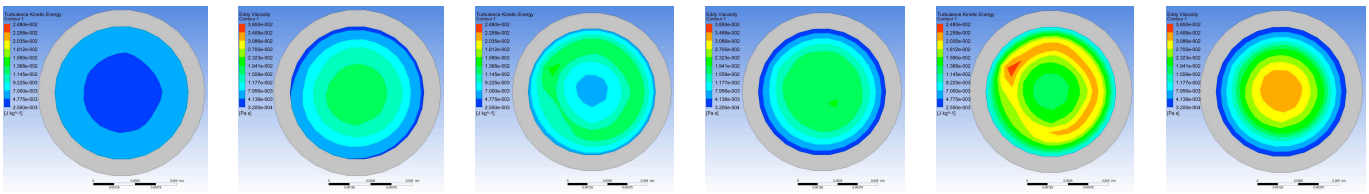
A B C D E F

Figure 3. Cross-sectional temperature distribution and velocity contours of water and xanthan gum solutions at Re = 10,000 and 50 °C: (**A**) temperature distribution of water, (**B**) velocity contour of water, (**C**) temperature distribution of XG 100 ppm, (**D**) velocity contour of XG 100 ppm, (**E**) temperature distribution of XG 300 ppm, and (**F**) velocity contour of XG 300 ppm.

A similar difference was observed in the temperature contours. In both cases, the highest temperature appeared near the heated wall, and the lowest temperature remained in the pipe core, which is consistent with the imposed constant heat flux boundary condition. Nevertheless, the temperature distribution of the xanthan gum solution differed from that of water, suggesting that the polymer addition also influenced the thermal transport process inside the pipe [30].

These contour distributions confirm that the hydraulic and thermal responses are strongly governed by the near-wall region, where both momentum and heat-transfer gradients are concentrated. This observation provides the physical basis for the subsequent discussion on pressure drop, friction factor, drag reduction, Nusselt number, and heat-transfer reduction.

To further examine the turbulence-related flow characteristics, Figure 4 presents the cross-sectional contours of the eddy viscosity and turbulent kinetic energy for water, XG 100 ppm, and XG 300 ppm at Re = 10,000 and 50 °C. The eddy viscosity contours indicate the distribution of turbulent momentum diffusion, while the turbulent kinetic energy contours represent the intensity of turbulence predicted by the *SST k–ω* model. Compared with water, the xanthan gum solutions show modified turbulence distributions across the pipe section, indicating that polymer addition alters the near-wall momentum transport. The XG 300 ppm case exhibits a more pronounced change in the turbulence field than the XG 100 ppm case, which supports the stronger but more condition-dependent drag-reduction behaviour observed at higher concentrations.



A B C D E F

Figure 4. Cross-sectional contours of turbulent kinetic energy and eddy viscosity for water and xanthan gum solutions at Re = 10,000 and 50 °C: (**A**) turbulent kinetic energy of water, (**B**) eddy viscosity of water, (**C**) turbulent kinetic energy of XG 100 ppm, (**D**) eddy viscosity of XG 100 ppm, (**E**) turbulent kinetic energy of XG 300 ppm, and (**F**) eddy viscosity of XG 300 ppm.

3.1. Drag Reduction Performance

Figure 5 presents the experimental and numerical drag reduction (DR) of xanthan gum solutions at 100 ppm and 300 ppm over the Reynolds number range of 8000–12,000 and

temperatures of 30 °C, 40 °C, and 50 °C. Overall, both approaches confirm that xanthan gum produces a positive drag-reduction effect under all investigated conditions [31–34]. However, the magnitude of DR depends on the concentration and temperature, while the experimental results show a wider variation than the numerical predictions.

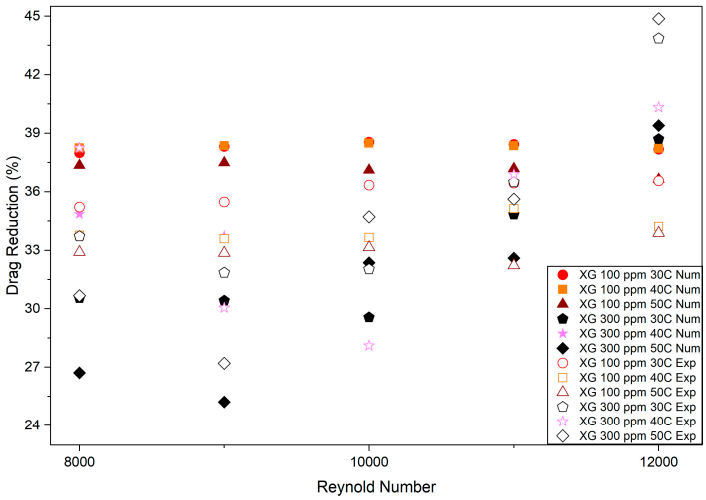


Figure 5. Comparison of experimental and numerical drag reduction in xanthan gum solutions at 100 ppm and 300 ppm as a function of Reynolds numbers at 30 °C, 40 °C, and 50 °C.

For the 100 ppm solution, the numerical results show a relatively stable DR level across the investigated Reynolds numbers, particularly at 30 and 40 °C. The predicted values remain within a narrow range, indicating that the low-concentration xanthan gum solution provides a consistent hydraulic benefit once turbulent flow is established. The experimental data follow the same general trend, although the measured values are slightly more scattered. This difference is expected because drag-reducing polymer flows are highly sensitive to pressure-drop measurement uncertainty, polymer distribution, and temperature-dependent rheological changes.

For the 300 ppm solution, the DR response becomes more condition-dependent. Compared with XG 100 ppm, the higher concentration produces a broader range of DR values, especially in the experimental data. At lower and intermediate Reynolds numbers, drag-reduction performance fluctuates, whereas at higher Reynolds numbers, particularly near Re = 12,000, the DR tends to increase markedly. This indicates that the stronger shear-thinning character of the 300 ppm solution can enhance turbulence attenuation under sufficiently intense flow conditions, although the response is less uniform than that of the 100 ppm solution.

The comparison between experimental and numerical data shows that the CFD model captures the main hydraulic behaviour of xanthan gum solutions, especially the consistently positive drag-reduction effect and the concentration-dependent change in DR response. Quantitative deviations remain, mainly for the 300 ppm solution, where polymeric turbulent flow is more sensitive to rheological representation and near-wall momentum transport. Therefore, Figure 5 demonstrates that xanthan gum drag reduction is governed not only by Reynolds numbers, but also by the coupled influence of polymer concentration, temperature-dependent rheology, and near-wall turbulence suppression.

3.2. Nusselt Number and Heat-Transfer Reduction

The experimental Nusselt number was estimated using the measured thermal response of the test section, while the numerical Nusselt number was obtained from the CFD-predicted wall heat flux and bulk fluid temperatures. The comparison is used to assess

whether the numerical model can reproduce the heat-transfer trend of water and xanthan gum solutions.

For the Newtonian baseline, the Nusselt number of water was compared with the classical Dittus–Boelter correlation ($Nu = 0.023\ Re^{0.8}\ Pr^{0.4}$), which is widely used for turbulent flow in smooth pipes [34].

Figure 6 compares the experimental and numerical Nusselt numbers of water and xanthan gum solutions at 100 ppm and 300 ppm over the Reynolds number range of 8000–12,000 and temperatures of 30 °C, 40 °C, and 50 °C. The Dittus–Boelter correlation graph is also included as a turbulent Newtonian reference, while the laminar constant-wall-temperature value of Nu = 3.66 and the Matthys correlation for polymer solution are shown for comparison.

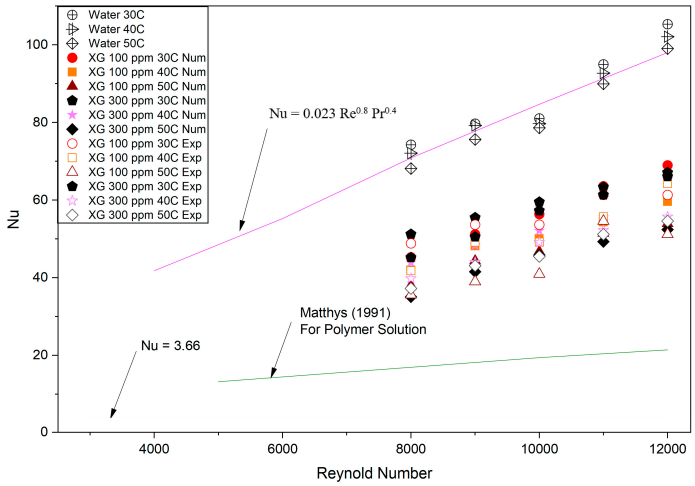


Figure 6. Variation in Nusselt numbers for water and xanthan gum solutions at 100 and 300 ppm at 30 °C, 40 °C, and 50 °C as a function of Reynolds numbers.

Water exhibits the highest Nusselt number under all investigated conditions, and its numerical trend follows the Dittus–Boelter correlation reasonably well. This agreement confirms that the numerical model can reproduce the expected turbulent heat-transfer behaviour of the Newtonian baseline. In contrast, both XG 100 ppm and XG 300 ppm show substantially lower Nusselt numbers than water, indicating that xanthan gum addition suppresses convective heat transfer.

The reduction in Nusselt number becomes more evident for the higher concentration. In general, XG 300 ppm produces lower thermal transport capability than XG 100 ppm, which can be attributed to stronger shear-thinning behaviour and greater damping of near-wall turbulent mixing. Although the Nusselt number still increases with the Reynolds number, the rate of increase is lower than that of water. This confirms that polymer-induced drag reduction is accompanied by a reduction in turbulent heat transport.

The comparison between experimental and numerical data shows that the CFD results capture the main trend of the measured Nusselt number, particularly the separation between water and xanthan gum solutions. Some deviations remain between experimental and numerical values, especially for the polymer solutions, due to the sensitivity of non-Newtonian heat transfer to rheological parameters, temperature control, and near-wall turbulence modelling. Overall, Figure 6 demonstrates that xanthan gum improves hydraulic performance but reduces convective heat-transfer effectiveness.

Figure 7 shows the experimental and numerical heat-transfer reduction (HTR) of xanthan gum solutions at 100 ppm and 300 ppm over the Reynolds number range of 8000–12,000 at 30 °C, 40 °C, and 50 °C. All cases exhibit positive HTR values, confirming

that xanthan gum reduces convective heat transfer relative to water. Compared with the drag-reduction trend, the HTR response shows a larger variation, indicating that thermal performance is more sensitive to the Reynolds number, temperature, and polymer concentration.

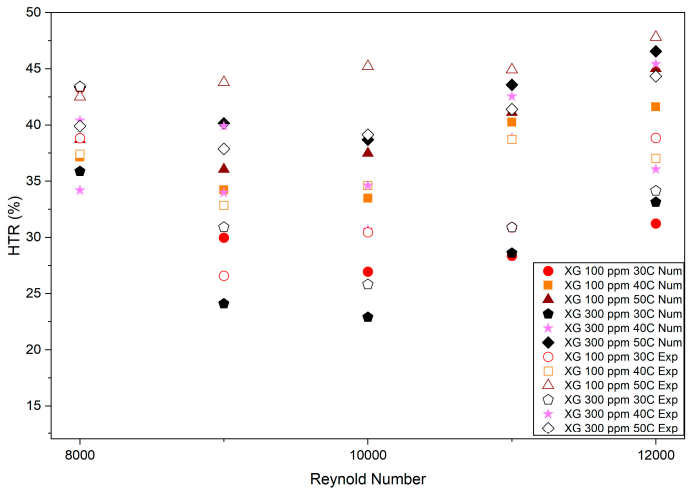


Figure 7. Experimental and numerical heat-transfer reduction in xanthan gum solutions at 100 ppm and 300 ppm as a function of Reynolds numbers at 30 °C, 40 °C, and 50 °C.

For XG 100 ppm, both numerical and experimental results show a moderate heat-transfer penalty. The HTR values fluctuate with the Reynolds number, suggesting that the thermal response is governed by the competition between turbulence intensification at higher Reynolds numbers and polymer-induced suppression of near-wall turbulent transport. For XG 300 ppm, the HTR values are generally higher, particularly at elevated Reynolds numbers and temperatures. This indicates that increasing the xanthan gum concentration strengthens the damping of turbulent thermal transport, resulting in a greater reduction in convective heat transfer.

The comparison between experimental and numerical data shows that the model captures the main thermal trend, especially the consistently positive HTR and the stronger heat-transfer penalty at higher concentrations. However, the experimental data display a wider scatter, which may be associated with temperature-control uncertainty, pressure and temperature measurement sensitivity, and the simplified rheological representation used in the numerical model.

3.3. Relationship Between Drag Reduction and Heat Dissipation Ratio

Figure 8 shows the relationship between drag reduction (DR) and heat-transfer reduction (HTR) for xanthan gum solutions at 100 ppm and 300 ppm based on both experimental and numerical results. This comparison is important because the performance of a drag-reducing polymer solution cannot be evaluated only from its ability to reduce pressure loss. A higher DR is beneficial for hydraulic efficiency, but a higher HTR indicates deterioration of convective heat transfer. Therefore, the preferred operating condition is located toward the upper-left region of the plot, where high drag reduction is achieved with a relatively low heat-transfer penalty.

For XG 100 ppm, the DR values are relatively stable within a narrow range, while the HTR values vary more widely. This indicates that the low-concentration solution provides a consistent hydraulic benefit, although its thermal penalty remains dependent on the temperature and Reynolds number. In contrast, XG 300 ppm shows a broader distribution of both DR and HTR. Some cases produce higher DR than XG 100 ppm, but this improvement is often accompanied by higher HTR. This confirms that increasing the

xanthan gum concentration can enhance drag-reduction performance, but it also increases the risk of heat-transfer deterioration.

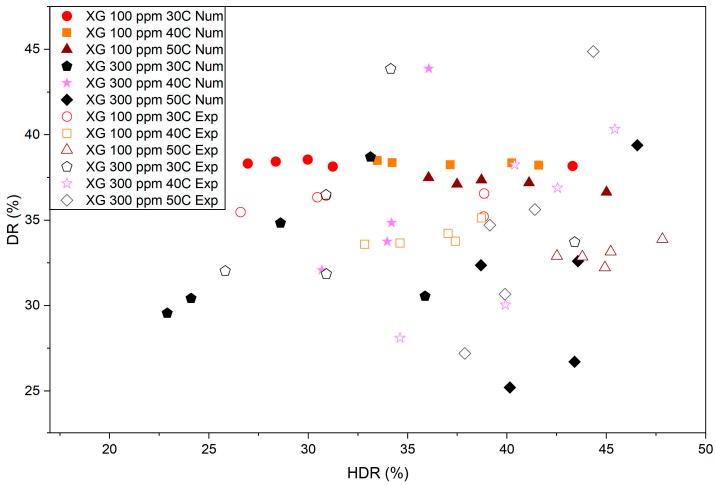


Figure 8. Relationship between heat dissipation ratio (HDR) and drag reduction (DR) of xanthan gum solutions at 100 and 300 ppm at 30 °C, 40 °C, and 50 °C.

The experimental data exhibit greater scatter than the numerical results, particularly for XG 300 ppm. This behaviour reflects the higher sensitivity of concentrated polymer solutions to rheological variation, temperature control, and near-wall turbulent transport. Nevertheless, both datasets show the same general tendency: xanthan gum addition produces a coupled hydraulic–thermal response, where drag reduction and heat-transfer reduction occur simultaneously.

Overall, Figure 8 confirms that the optimum xanthan gum concentration should not be determined solely from the maximum DR value. Although XG 300 ppm may provide stronger drag reduction under certain conditions, XG 100 ppm offers a more stable compromise between pressure-loss reduction and heat-transfer penalty. Thus, the selection of xanthan gum concentration should depend on the design priority of the system, whether hydraulic efficiency or heat-transfer performance is more critical.

4. Conclusions

This study experimentally and numerically investigated the hydraulic and thermal behaviour of xanthan gum solutions at 100 ppm and 300 ppm in turbulent smooth pipe flow at 30–50 °C and Re = 8000–12,000. Both concentrations produced positive drag reduction relative to water. The XG 100 ppm solution showed a more stable drag-reduction response, with DR generally ranging from approximately 31% to 39%, while XG 300 ppm showed a wider and more condition-dependent range of about 25% to 45%, with higher values observed at higher Reynolds numbers.

The numerical results captured the main experimental trend, although deviations were more evident for XG 300 ppm, indicating greater sensitivity to rheological variation and near-wall turbulence modelling. From the thermal perspective, water showed higher Nusselt numbers of approximately 68–106. In contrast, XG 100 ppm produced Nusselt numbers of approximately 45–69, while XG 300 ppm showed lower values of about 35–61. The corresponding heat-transfer reduction ranged from approximately 26% to 48% for XG 100 ppm and from approximately 23% to 46% for XG 300 ppm. These results confirm that drag reduction was accompanied by a thermal penalty. Overall, increasing xanthan gum concentration can enhance hydraulic performance, but it also intensifies heat-transfer deterioration; therefore, the optimum concentration should be selected based on the balance between pressure-loss reduction and acceptable thermal performance.

Author Contributions: A.C.I.: Conceptualization, methodology, simulation, formal analysis, data curation, and writing—original draft. S.P.S.: Supervision, validation, and writing—review and editing. G.: Supervision, investigation, technical discussion, and validation. Y.: Supervision, conceptual guidance, and writing—review and editing. All authors have read and agreed to the published version of the manuscript.

Funding: This research was supported by the collaboration between the Faculty of Engineering, University of Indonesia and Gunadarma University No specific grant number was assigned for this support. The APC was funded by Gunadarma University.

Institutional Review Board Statement: Not applicable, as this study did not involve humans or animals.

Informed Consent Statement: Not applicable, as this study did not involve humans.

Data Availability Statement: The data supporting the findings of this study are available upon reasonable request from the corresponding author.

Acknowledgments: The authors gratefully acknowledge the collaboration between the Faculty of Engineering University of Indonesia and Gunadarma University in supporting this research. The authors also appreciate the academic support and computational facilities that contributed to the successful completion of this study.

Conflicts of Interest: The authors declare that they have no conflicts of interest regarding the publication of this paper.

References

1. Sigalotti, L.D.G.; Guzmán, E. An overview of viscous and highly viscous fluid flows in straight and elbow pipes: I—Single-phase flows. *Fluids* **2025**, *10*, 125. [CrossRef]
2. Serafini, F.; Battista, F.; Gualtieri, P.; Casciola, C.M. Drag reduction in polymer-laden turbulent pipe flow. *Fluids* **2022**, *7*, 355. [CrossRef]
3. Dubief, Y.; Terrapon, V.E.; Hof, B. Elasto-inertial turbulence. *Annu. Rev. Fluid Mech.* **2023**, *55*, 675–705. [CrossRef]
4. Hong, C.H.; Choi, S.J.; Cho, Y.I.; Choi, H.J. Effect of salt on turbulent drag reduction of xanthan gum. *Carbohydr. Polym.* **2015**, *121*, 342–347. [CrossRef]
5. Kadhim, B.J.; Mahdy, O.S.; Alsaedi, S.S.; Majdi, H.S.; Shnain, Z.Y.; Alwaiti, A.A.; AbdulRazak, A.A. Effect of rigid xanthan gums (RXGs) on flow and pressure drops to improve drag reduction rates in horizontal pipe flow. *ChemEngineering* **2023**, *7*, 36. [CrossRef]
6. Chang, A.; Huang, L.; Wei, S.; Shao, M. Analysis of the drag reduction performance and rheological properties of drag-reducing additives. *Polymers* **2024**, *16*, 1247. [CrossRef]
7. Choppe, E.; Puaud, L.; Nicolai, P. Rheology of xanthan solutions as a function of temperature, concentration, and ionic strength. *Carbohydr. Polym.* **2010**, *82*, 1228–1235. [CrossRef]
8. Reinoso, D.; Martín-Alfonso, M.; Luckham, P.; Martínez-Boza, F. Rheological characterisation of xanthan gum in brine solutions at high temperature. *Carbohydr. Polym.* **2019**, *203*, 103–109. [CrossRef]
9. Brunchi, C.E.; Morariu, S.; Iftime, M.M.; Stoica, I. Xanthan gum in solution and solid-like state: Effect of temperature and polymer concentration. *J. Mol. Liq.* **2023**, *387*, 122600. [CrossRef]
10. Zhang, Y.; Zhou, F.; Kang, J. Flow and heat transfer in drag-reducing polymer solution. *Appl. Therm. Eng.* **2020**, *174*, 115185. [CrossRef]
11. Shojaeian, M.; Karimzadehkhouei, M.; Koşar, A. Experimental investigation on convective heat transfer of non-Newtonian flows of xanthan gum solutions in microtubes. *Exp. Therm. Fluid Sci.* **2017**, *85*, 305–312. [CrossRef]
12. Zhang, H.; Kang, Y.; Xu, T. Study on heat transfer of non-Newtonian power-law fluid in pipes with different cross sections. *Procedia Eng.* **2017**, *205*, 3381–3388. [CrossRef]
13. Said, M.; Haq, B.; Al Shehri, D.; Rahman, M.M.; Muhammed, N.S.; Mahmoud, M. Modification of xanthan gum for a high-temperature and high-salinity reservoir. *Polymers* **2021**, *13*, 4212. [CrossRef]
14. Wang, X.; Qiu, X.; Zhang, X.; Zhao, L.; Xi, Z. Effect of elasticity on heat and mass transfer of highly viscous non-Newtonian fluids flow in circular pipes. *Polymers* **2025**, *17*, 1393. [CrossRef] [PubMed]
15. Soares, E.J. Review of mechanical degradation and de-aggregation of drag reducing polymers in turbulent flows. *J. Non-Newton. Fluid Mech.* **2020**, *276*, 104225. [CrossRef]

16. Barbosa, K.C.; Cussuol, J.D.; Soares, E.J.; Andrade, R.M.; Khalil, M.C. Polymer drag reduction below and above the overlap concentration. *J. Non-Newton. Fluid Mech.* **2022**, *310*, 104942. [CrossRef]
17. Zhang, Y.; Rabenjafimanantsoa, A.H.; Skadsem, H.J. Interfacial dynamics of miscible displacement of shear-thinning fluid in a vertical channel. *Fluids* **2023**, *8*, 35. [CrossRef]
18. Cayeux, E. Calibration of thixotropic and viscoelastic shear-thinning fluids using pipe rheometer measurements. *Fluids* **2024**, *9*, 23. [CrossRef]
19. Kinra, S.; Pal, R. Pipe flow of suspensions of cellulose nanocrystals. *Fluids* **2023**, *8*, 275. [CrossRef]
20. Magnon, E.; Cayeux, E. Precise method to estimate the Herschel-Bulkley parameters from pipe rheometer measurements. *Fluids* **2021**, *6*, 157. [CrossRef]
21. ANSYS. *Fluent Theory Guide: Standard, BSL, and SST k-ω Models*; ANSYS Documentation: Canonsburg, PA, USA, 2020.
22. Habibpour, M.; Clark, P.E. Drag reduction behavior of hydrolyzed polyacrylamide/xanthan gum mixed polymer solutions. *Pet. Sci.* **2017**, *14*, 412–423. [CrossRef]
23. Ihmoudah, A.; Rahman, M.A.; Butt, S.D. CFD and experimental studies of yield power-law fluids in turbulent pipe flow. In Proceedings of the International Conference on Offshore Mechanics and Arctic Engineering, Tokyo, Japan, 7–12 June 2018; Volume 8. [CrossRef]
24. Ogata, S.; Nishina, Y.; Tochigi, H.; Watanabe, K. Drag reduction and heat transfer characteristics of graphene oxide nanosheet suspensions. *Trans. JSME* **2020**. [CrossRef]
25. Carravetta, A.; Fecarotta, O.; Martino, R.; Morani, M.C. Rheological characterization of non-Newtonian mixtures by pressure pipe tests. *Fluids* **2021**, *6*, 419. [CrossRef]
26. Behroyan, I.; Vanaki, S.M.; Ganesan, P.; Saidur, R. A comprehensive comparison of various CFD models for convective heat transfer of Al_2O_3 nanofluid inside a heated tube. *Int. Commun. Heat Mass Transf.* **2016**, *70*, 27–37. [CrossRef]
27. Sigalotti, L.D.G.; Alvarado-Rodríguez, C.E.; Rendón, O. Fluid flow in helically coiled pipes. *Fluids* **2023**, *8*, 308. [CrossRef]
28. Wang, S.; Gao, D.; Pouraria, H. Fluid–structure interaction effects on developing complex non-Newtonian flows within flexible tubes. *Fluids* **2025**, *10*, 210. [CrossRef]
29. Zhu, J. A new solution of drag for Newtonian fluid droplets in a power-law fluid. *Fluids* **2024**, *9*, 99. [CrossRef]
30. Di Giusto, D.; Marchioli, C. Turbulence modulation by slender fibers. *Fluids* **2022**, *7*, 255. [CrossRef]
31. Cheng, Z.; Zhang, P.; Wang, X.; Song, X.; Dai, X.; Gao, L.; Zhang, X.; Zhang, G.; Lu, Y. Drag reduction and degradation by sodium alginate in turbulent flow. *Sci. Rep.* **2024**, *14*, 16854. [CrossRef]
32. Cheng, Z.; Zhang, X.; Dai, X.; Zhai, H.; Song, X.; Wang, X.; Gao, L.; Zhang, G.; Lu, Y.; Li, L.; et al. Experimental study on the drag reduction performance of sodium alginate in saline solutions. *Sci. Rep.* **2024**, *14*, 32123. [CrossRef]
33. Watanabe, K.; Ogata, S. Drag reduction by dried malted rice solutions in pipe flow. *Liquids* **2024**, *4*, 432–442. [CrossRef]
34. Bergman, T.L.; Lavine, A.S.; Incropera, F.P.; DeWitt, D.P. *Fundamentals of Heat and Mass Transfer*, 7th ed.; John Wiley & Sons: Hoboken, NJ, USA, 2011.

Disclaimer/Publisher's Note: The statements, opinions and data contained in all publications are solely those of the individual author(s) and contributor(s) and not of MDPI and/or the editor(s). MDPI and/or the editor(s) disclaim responsibility for any injury to people or property resulting from any ideas, methods, instructions or products referred to in the content.